Journal Name

RSCPublishing

ARTICLE

System-level network simulation for robust centrifugal-microfluidic lab-on-a-chip systems – Electronic supplement

Cite this: DOI: 10.1039/x0xx00000x

I. Schwarz[a], S. Zehnle[a], T. Hutzenlaub[a,b], R. Zengerle[a,b,c], N. Paust[a,b]

Received 00th January 2012,
Accepted 00th January 2012

DOI: 10.1039/x0xx00000x

www.rsc.org/

S1 Curved channel simulation

S 1.1 Equivalent modelling of curved channels

In order to model curved channels through lumped models of radial and isoradial channels, the pressures generated by the models need to match as closely as possible. To this end, one procedure to determine the position & geometry parameters of the equivalent radial and isoradial channels is as follows:

The curved channel of interest is divided in channel sections which are modelled separately and connected to represent the full curved channel. In each of the channel sections, the radius and angle coordinate of the curved channel need to change monotonously. Each of such channel section is modelled by one radial and one isoradial channel model. In order to yield identical centrifugal pressures when filled with liquid, the radial position and extension of each curved channel section needs to be identical to the radial position and extension of the corresponding equivalent radial channel model. In order to yield identical viscous dissipation of the equivalent channel models, the length of the isoradial channel model is chosen such that the total length of the curved channel section is identical to the sum of the lengths of the equivalent radial and the isoradial channel.

The errors introduced with this procedure are:

a) The Euler pressure calculated in the equivalent channels is not identical to the Euler pressure in the real curved channel section.
b) The same liquid volume in partially filled curved channels and in the corresponding equivalent channel models may lead to a small deviation in hydrostatic pressure.
c) Both errors lead to deviations between the filling dynamics of curved and equivalent channels as pressure contributions deviate from the values in the real curved channel during filling.

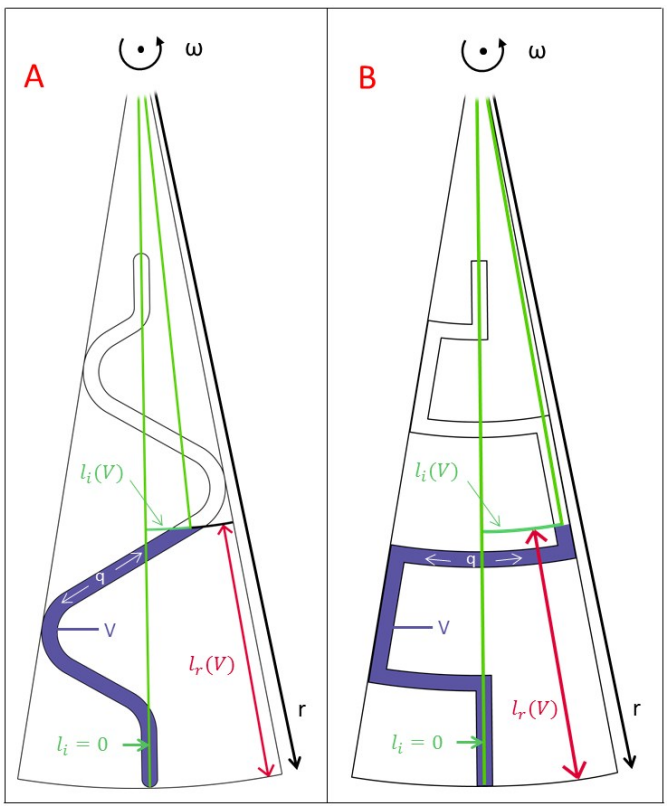

S-Figure 1: A) Illustration of a curved channel. The liquid filled radial length of the channel is indicated with $l_r(V)$ in red. The liquid filled isoradial length of the channel is indicated with $l_i(V)$ in green. Both lengths are functions of the liquid volume V in the channel – indicated in blue. **B)** Illustration of the equivalent representation of the curved channel through radial and isoradial channel segments. The liquid filled radial and isoradial lengths are indicated analogously to A for comparison. The volume dependencies of $l_r(V)$ and $l_i(V)$ are handled automatically by the radial and isoradial channel segment models. A procedure for choosing appropriate dimensions of the equivalent channel segments is described in the main text.

If these deviations can be neglected, the equivalent channel models yield a good representation of the fluidic behavior of the curved channel network behavior. If on the other hand these deviations are not acceptable the implementation of a full model of a curved channel is necessary.

S 1.1 Direct modelling of curved channels

Due to the potentially complex shapes of curved channels, the pressure terms in the transfer function of a curved channel model need to be expressed in terms of fill volume dependent functions. For a given cross section of a curved channel, the pressures can be calculated based on the liquid filled radial distance $l_r(V)$ and the liquid filled isoradial distance $l_i(V)$ as illustrated in S-Figure 1 for a partially liquid filled curved channel. The corresponding relations are listed in S-Table 1.

S-Table 1: Considered physical effects in curved channel models. **ρ** denotes the density of the considered liquid. **r** stands for the radial distance from the centre of rotation to the most distant point of the curved channel. ***ω*** denotes the angular spin frequency of the considered disc. The liquid filled length $l = \frac{V}{A}$ inside a channel is given by with the liquid volume V and the cross sectional area A of the channel. The projections of ***l*** on the radial and isoradial directions as a function of *V* are given by $l_r(V)$ and $l_i(V)$. The value of $l_i(0)$ is chosen to 0. The flow rate through a channel is ***q***. The width and depth of a rectangular channel are specified by **w** and **d**, respectively. The fluidic resistance $\mathbf{R_f}$ depends on the shape of the cross-section of the channel as indicated by $\mathbf{C_g}$. For the liquids, the dynamic viscosity and surface-tension are specified by **η** and **σ.** For the case that different materials are used for the walls of a rectangular channel, θ_1 and θ_2 specify the contact angles at the channel walls that are separated by the distance **w** and θ_3 and θ_4 specify the contact angles at the channel walls that are separated by the distance **d.**

Centrifugal pressure	$p_{cent} = \frac{\rho}{2}\omega^2\left(r^2 - \left(r - l_r(V)\right)^2\right)$
Euler pressure	$p_{euler} = \rho\, G_E(V)\frac{d\omega}{dt}$ $G_E(V) = \int_0^V \left(r - l_r(V)\right)\frac{dl_i(V)}{dV}dV$
Inertial pressures	$p_{inert} = \frac{\rho\, V\, dq}{A^2\, dt}$
Viscous dissipation	$p_{visc} = R_f\, q$, with $R_f = C_g\frac{\eta\, V}{A^3}$ Square cross section: $C_g = 28.4$ Rectangular cross section: $C_g = \frac{12}{\frac{d}{w}\left(1 - \frac{192\, d}{\pi^5\, w}\left(\tanh\frac{\pi\, w}{2\, d} + \frac{31}{32}\zeta(5) - 1\right)\right)}$ Geometry factors for trapezoidal and other cross-sections can be found in[1,2]
Capillary pressures	$p_{cap} = \sigma\left(\frac{\cos(\theta_1) + cos(\theta_2)}{w} + \frac{\cos(\theta_3) + cos(\theta_4)}{d}\right)$

The centrifugal pressure in a curved channel only depends on the liquid filled radial distance $l_r(V)$. Therefore, the centrifugal pressure is modelled by

$$p_{cent} = \frac{\rho}{2}\omega^2\left(r^2 - \left(r - l_r(V)\right)^2\right)$$

The function $l_r(V)$ can be obtained – analogously to the $h(V_{liquid})$ functions for chambers – from the CAD model by a series of cuts of the curved channel geometry at different radial distances and a fit of the resulting series of data points (radius, channel volume).

The Euler pressure term is more intricately linked to the geometry of the curved channel. As the Euler pressure of an isoradial channel depends on both, its radius and its length, the generalized geometry function for the Euler pressure in a curved channel $G_E(V)$ is given by

$$G_E(V) = \int_0^V \left(r - l_r(V)\right)\frac{dl_i(V)}{dV}dV$$

The needed function for the isoradial liquid filled channel length $l_i(V)$ can be obtained from the CAD model of the curved channel by fitting a sufficiently large set of (isoradial channel length, channel volume) data points. With both functions, $l_r(V)$ and $l_i(V)$, $G_E(V)$ can be calculated by numerical integration. Using $G_E(V)$, the Euler pressure component of the transfer function is calculated to

$$p_{euler} = \rho\, G_E(V)\frac{d\omega}{dt}$$

Inertial pressure and viscous dissipation only depend on the liquid filled length of the curved channel. Therefore, with a constant cross section with area A, the inertial pressure in a curved channel is given by

$$p_{inert} = \frac{\rho\, V\, dq}{A^2\, dt}$$

and the viscous dissipation is given by

$$p_{visc} = C_g\frac{\eta\, V}{A^3}q$$

with a geometry dependent factor C_g.

Effects that are not considered by this modelling scheme are flow resistance variations due to secondary flow transversal to the channel flow direction. These can be caused by the Coriolis force in arbitrary channels under rotation or by Dean flow in channel curves.

S2 Contact angle hysteresis

The effect of contact angle hysteresis describes that the contact angle between a liquid/gas interface and e.g. a channel wall is dependent on the direction of flow, i.e. whether a liquid is

wetting or de-wetting a surface. In the following, we will distinguish between liquids that do not permanently change the contact angle between liquid and substrate upon contact and liquids where this is the case – called "coating liquids". An example for such a coating liquid is blood plasma which can generate a surface layer of deposited protein on polymer substrates upon contact[3]. Because capillary pressures in chambers are small compared to capillary pressures in channels, the effect of capillary hysteresis is currently only implemented for channels and will be discussed on their example.

S 2.1 Non-coating liquids

For non-coating liquids, the effect of contact angle hysteresis can be modelled in channel models by use of two contact angles and a linear interpolation between the corresponding capillary pressures as illustrated in S-Figure 1. To implement the interpolation, an internal variable V_{cap} and an appropriately chosen parameter $V_{cap\,max}$ are introduced that allow to track the direction of flow. The variable V_{cap} integrates the liquid flow in a channel. The integration is stopped if the value of V_{cap} exceeds the interval $[-V_{cap\,max}, V_{cap\,max}]$. Therefore, $V_{cap}/V_{cap\,max}$ can be used as a linear interpolation variable between the capillary pressures of an advancing and a receding contact angle. Because the sign of the capillary pressure in a channel depends on the direction from which it is partially filled, two separate equations for the capillary pressure interpolation are implemented. The correct equation is chosen dependent on the wetting state signals of the channel. In the case depicted in S-Figure 1 where $V_{cap}/V_{cap\,max} = 1$ corresponds to a filling of a channel, the capillary pressure is determined by:

$$p_{cap\,hyst} = \frac{1}{2}\left(\frac{V_{cap}}{V_{cap\,max}} + 1\right) * p_{cap\,adv} - \frac{1}{2}\left(\frac{V_{cap}}{V_{cap\,max}} - 1\right) * p_{cap\,rec} \quad (1)$$

If otherwise the filling of a channel corresponds to $V_{cap}/V_{cap\,max} = -1$, the capillary pressure is determined by:

$$p_{cap\,hyst} = \frac{1}{2}\left(\frac{V_{cap}}{V_{cap\,max}} - 1\right) * p_{cap\,adv} - \frac{1}{2}\left(\frac{V_{cap}}{V_{cap\,max}} + 1\right) * p_{cap\,rec} \quad (2)$$

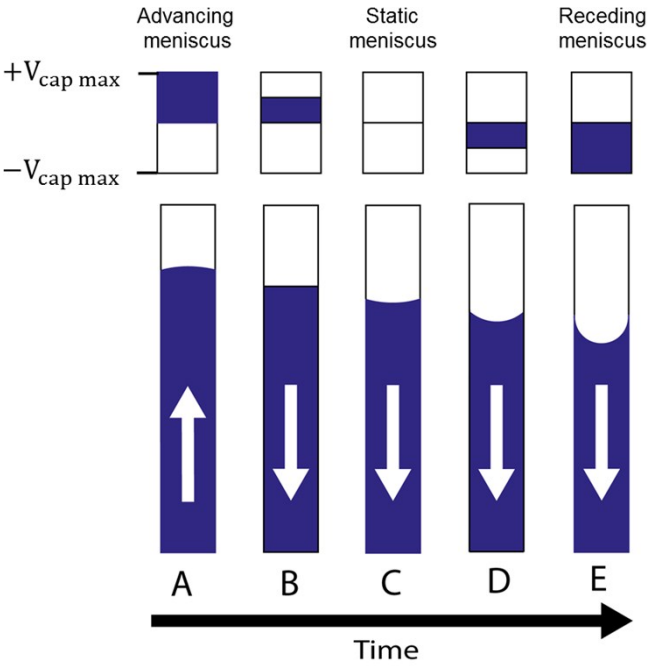

S-Figure 1: Illustration of the capillary hysteresis model implemented in channel models. The top part of the illustration indicates the value of the interpolation variable V_{cap}, the bottom part shows the liquid fill level and the meniscus curvature in a radially oriented channel together with the direction of liquid flow in each instance. **A:** liquid is flowing from bottom to top and the variable V_{cap}, indicates that the advancing contact angle applies. **B:** The liquid flow has reversed and the value of V_{cap} has decreased to 0.5. This leads to a capillary pressure of $3/4p_{cap\,adv} + 1/4p_{cap\,rec}$. **C&D:** The reversed liquid flow leads to a further decrease in V_{cap} which shifts the capillary pressure further to $p_{cap\,rec}$. **E:** The capillary pressure has reached $p_{cap\,rec}$.

S 2.2 Coating liquids

In the case of coating liquids each model block keeps track of the positions that have been in contact with liquid during the simulated fluid movements via an internal variable.

If liquid advances through a channel that was previously not in contact with liquid, the advancing contact angle between liquid and unchanged substrate applies. If otherwise a meniscus propagates into a channel that previously was in contact with the liquid, the changed contact angle between liquid and coated substrate applies. In case of a partially coated channel an interpolation between coated and uncoated contact angle is performed if a meniscus propagates from the coated to the uncoated channel part. This interpolation is analogous to the capillary hysteresis interpolation described in the previous section S 2.1. Therefore, for coating liquids two advancing contact angles and one receding contact angle exist. The interpolation between advancing and receding contact angle is performed as described in S 2.1 and the advancing contact angle that applies in any given moment is determined based on the wetting history of the channel.

S3 Capillary pressure interpolation at model block boundaries

As described in "wetting states and phase information propagation", capillary pressure interpolation at the interface between model blocks is necessary to avoid pressure jumps that would lead to solver instabilities during network simulation. Such jumps need to be avoided in each individual model block as it is impossible to precisely compensate the jump in one model block with an opposite jump in another model block. Therefore, during the transition of a liquid meniscus from one model block to the next, the capillary pressures of the two adjacent blocks need to be interpolated concurrently between zero and their start/end pressures. For the interpolation, an appropriate distance parameter d_{cap} is chosen. If the distance between the liquid/gas interface and the boundary of the modelled channels is smaller than d_{cap}, the adjacent model block is provided with the information about the position of the meniscus through an outgoing meniscus tracking signal $MenT_{out}$ and the capillary pressure is interpolated. To illustrate this, we discuss the interpolation process on the example given in S-Figure 2.

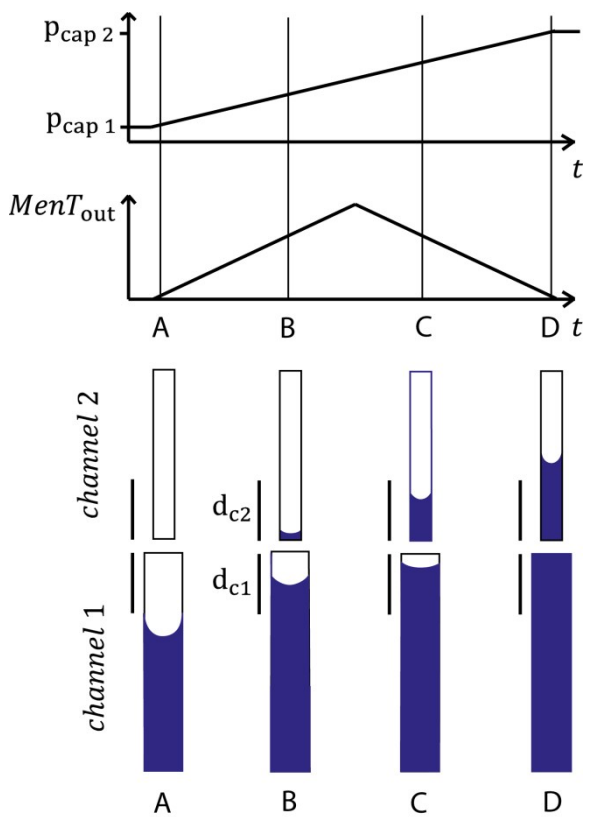

S-Figure 2: Illustration of the capillary pressure interpolation process on the example of two adjacent radially oriented channels. For illustration purposes, the shown curved menisci in the channels reflect the capillary pressure contribution in the respective channel – not the actual filling level. I.e. the indicated meniscus in step **B** does not indicate that liquid is actually in channel 2 but that the capillary pressure in channel 2 is being ramped up in the process of the capillary interpolation. Analogously, the indicated meniscus in **C** indicates the ramp-down of the capillary pressure in channel 1 which is full in that instance. The steps **A**-**D** of capillary interpolation are explained in the main text.

In **A**, *channel 1* is partially filled, and the distance between the liquid gas interface and the boundary to the empty *channel 2* is larger than d_{cap}. In this case, the capillary pressure in *channel 1* is at the value given by the capillary pressure hysteresis model and the capillary pressure in the empty *channel 2* is zero. This corresponds to a value of zero for the outgoing meniscus tracking signal $MenT_{out\,1}$ of *channel 1*.

B) The liquid has propagated towards the boundary between *channel 1* and *channel 2*. Here, the distance between the liquid/gas interface and the channel boundary is smaller than d_{cap}. In this case, the meniscus position information is propagated from *channel 1* to *channel 2* via: $MenT_{out\,1} = 1 - (L - l_{fill})/d_{cap}$, where L is the length of *channel 1* and l_{fill} is the liquid filled length of *channel 1*. With this, $MenT_{out\,1}$ starts from zero when the meniscus reaches the distance d_c from the channel boundary and increases linearly to 1 when the meniscus reaches the channel boundary. During this phase, the capillary pressure in *channel 1* is calculated to

$$p_{cap\,1} = p_{cap\,hyst\,1} * \frac{1}{2}(2 - MenT_{out\,1})$$

At the same time, the capillary pressure in *channel 2* is calculated to

$$p_{cap\,2} = p_{cap\,hyst\,2} * \frac{1}{2}(MenT_{out\,1})$$

It is important to note that the capillary pressure calculation of *channel 1* is performed in the wetting state of a partially filled channel. Therefore, the information of the filling level is directly available to the model of *channel 1*. *Channel 2* on the other hand is empty, thus no direct information about the position of the meniscus is available. Through the $MenT_{out}$ signal of *channel 1* ($MenT_{out\,1}$) *channel 2* is capable of interpolating its capillary pressure to half the maximum value, while the meniscus is approaching the boundary between *channel 1* and *2* from the side of *channel 1*.

C) The meniscus has crossed the boundary between *channel 1* and *channel 2*. As described in "wetting states and phase information propagation", the following exchange of wetting state signals happened between **B** and **C:** *Channel 1* sent the wetting state signal 1 – for wet – to *channel 2*. *Channel 2* thus changed its wetting state to "filling" and propagated the wetting state signal 1 back to *channel 1*. With this wetting state signal, *channel 1* registered that it is now in the wetting state "full". In situation **C,** the information about the meniscus position is therefore directly available to *channel 2* and *channel 1* receives the meniscus tracking signal $MenT_{out\,2}$ from *channel 2*. The capillary pressure in *channel 1* is now calculated according to the wetting state "full":

$$p_{cap\,1} = p_{cap\,hyst\,1} * \frac{1}{2}(MenT_{out\,2})$$

The capillary pressure in *channel 2* is calculated according to the wetting state "filling":

$$p_{cap\,2} = p_{cap\,hyst\,2} * \frac{1}{2}(2 - MenT_{out\,2})$$

D) The meniscus has propagated further into *channel 2*. As the distance between gas/liquid interface and meniscus boundary is

larger than d_{cap}, the meniscus tracking signal $MenT_{out\,2}$ is zero. This leads to a capillary pressure of zero inside *channel 1* and the full capillary pressure of the hysteresis model in *channel 2*.

This procedure is used for all connections between model blocks and allows for capillary self-priming or capillary de-wetting in microfluidic networks – dependent on the contact angles of the liquids/channels and their initial filling conditions. The chosen dimension for d_{cap} in this work was 20 µm for all model blocks.

S4 T-junction model implementation

T junctions are indispensable as they are a prerequisite of true microfluidic networks. As commercially available network simulation solvers are readily capable of handling the flow division at a branching point according to Kirchhoff's law. The challenge is the handling of two phase flows. To achieve a correct description of the propagation of the interfaces in the T-junction including capillary pressures, a T-junction model consists of four elements. Three of these elements are modified channel models that allow for the handling of the capillary pressure interpolation. In order to avoid confusion with normal channel models, the channel models that belong to the T-junction model are named branches. Because the branches are a part of the T-junction model and not intended to contribute viscous dissipation, their parameters for the cross sections were chosen in this work to the largest of the cross sections of the connected channels and their length to 100 µm. The fourth element is a T-junction logic model that handles the signal propagation between the branches. In the following, we discuss first the propagation of the wetting state information through the T-junction model and later the additional issues that are involved with the robust handling of capillary pressures in T-junctions.

S 4.1 Wetting state information transmission

The procedure for liquid/gas interface propagation from one model block to the next has been described in "wetting states and phase information propagation" in the paper as well as in "S2 Capillary pressure interpolation at model block boundaries" in the electronic supplement. When a liquid/gas interface is propagated from a model block through a T-junction to other connected model blocks, the liquid gas/interface is first propagated to one branch of the T-junction. The wetting state information propagation at this point is identical to the already discussed block to block propagation (but not the capillary pressure handling – see next section). The next liquid/gas interface propagation is from one branch to the two adjacent branches (the developed model does currently not handle the conceivable case of an interface propagation from one branch to only one of the two connected branches). The wetting state signal transmission to perform the liquid/gas interface propagation is thereby handled by the (T-junction-) logic block. After this interface propagation step is completed, the propagation to the model blocks connected to the second and third branch again follows the block to block propagation procedure.

To allow for the logic block to choose the correct logical case for the wetting state propagation, the logic block receives the wetting state signals not only from the side on which the three branches are connected together (proximal side) but also from the side that is connected to the model blocks that are to be linked via the T-junction model (distal side).

Without limitation of generality, we discuss the process of liquid/gas interface propagation from one branch to the two others for the case of an empty T-junction getting filled – see S-Figure 2 and S-Table 2. The opposite case of a full T-junction being emptied is implemented analogously.

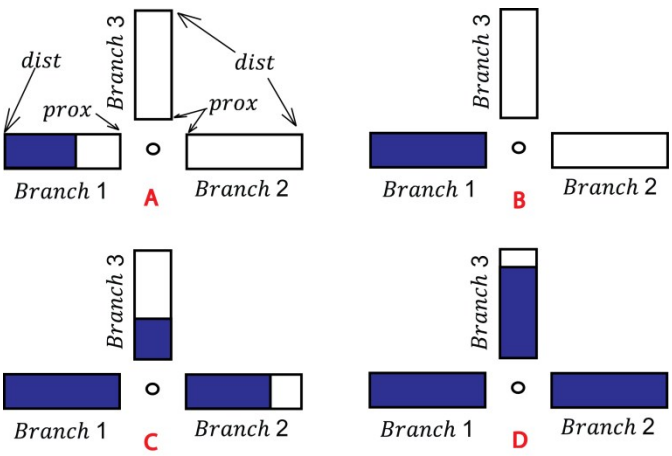

S-Figure 2: Illustration of the fluidic filling process of a T-junction. The branches of a T-junction model are depicted for the process of filling from the left side. The logic block is indicated as the circle in the center. The processes involved with the filling steps **A**-**D** are explained in the main text.

In step **A** the liquid/gas interface is in *branch 1*. Therefore, the provided wetting state signals of the branches lead to the wetting state "filling from *branch 1*" in the logic block – see S-Table 2.

S-Table 2: Table of wetting states and wetting state signals for the branches and the logic block of a T-junction model during the process of filling. The instances **A**-**D** correspond to the instances depicted in S-Figure 2.

Signal	**A**	**B**	**C**	**D**
$wet_{out\,dist\,1}$	1	1	1	1
$wet_{out\,dist\,2}$	0	0	0	1
$wet_{out\,dist\,3}$	0	0	0	0
$wet_{out\,prox\,1}$	0	1	1	1
$wet_{out\,prox\,2}$	0	0	1	1
$wet_{out\,prox\,3}$	0	0	1	1
Wetting states	**A**	**B**	**C**	**D**
Branch 1	Filling	Full	Full	Full
Branch 2	Empty	Empty	Filling	Full
Branch 3	Empty	Empty	Filling	Filling
Logic block	Filling 1	Filling 1	Filling 2&3	Filling 3

In this state, the logic block sends the wetting state signal 0 (dry) to the proximal connections of the branches and propagates the meniscus tracking variable $MenT_{out\,1}$from *branch 1* to the *branches 2 and 3*.

In step **B**, *branch 1* has been filled and sends the wetting state signal 1 (wet) to the *logic block*. This signal is passed on by the *logic block* to the *branches 2 and 3*. This is the status indicated in S-Table 2 **B**. The two branches therefore change their wetting state from empty to filling and propagate their proximal wetting state 1 (wet) back to the logic block. Once both branches consistently send this signal, the wetting state of the *logic block* changes to "*branch 1* full, *branches 2 & 3* filling" – i.e. the state indicated in S-Table 2 **C**. In this state, the *logic block* sends the wetting state signal 1 (wet) to all branches and propagates the average of the meniscus tracking signals $MenT_{out\,2}$and $MenT_{out\,3}$ to *branch 1*. In S-Figure 2 **C**, the liquid in the *branches 2 & 3* has propagated, but due to differences in the flow rate, *branch 2* is filled further than *branch 3*. In **D**, this leads to the case where the *branches 1 & 2* are filled and *branch 3* is still in the process of filling. This state is analogous to the initial state with *branch 1* partially filled. Therefore, the logic block propagates the meniscus tracking signal $MenT_{out\,3}$ to the *branches 1 & 2* and also sends the wetting state signal 1 to all three branches.

This exemplary filling process is implemented symmetrically so that filling or emptying may occur from any branch. The T-junction model is capable of handling liquid propagation as long as no flow conditions prevail, that would lead to the formation of bubbles or plugs, i.e. if liquid is injected from one branch and gas from a second branch. As the presented network simulation models are not designed to handle more than one concurrent liquid/gas interface per model block such conditions would also directly lead to invalid simulation results in the remaining network. Therefore, the T-junction does not consider cases for such flow conditions and they need to be avoided to obtain valid simulation results.

S 4.2 Capillary pressure handling

As we have seen in the previous section "S2 Capillary pressure interpolation at model block boundaries", the capillary pressure in a filled or empty model block depends on the position of the liquid/gas interface in an adjacent partially filled model block. In a T-junction model, the cases where one branch has just filled and the two adjacent branches are filled within the interpolation distance leads to the question what meniscus position signal to provide to the already full branch. The simple approximation used in the implemented model is to take the average of the meniscus position signals of the partially filled branches as input to the full branch. This procedure is also implemented accordingly for the symmetrical case of a filled T-junction emptying ifone branch is empty and the two adjacent branches are emptied within the capillary interpolation distance. This procedure allows to approximately maintain the overall capillary pressure during the interface propagation between branches in order to correctly describe capillary pressure driven wetting/de-wetting behavior in T-junctions. It is important to note that the capillary pressure interpolation between branches is necessary to avoid pressure discontinuities inside a given branch model block, although the branches have identical capillary pressures.

An additional complication for the liquid/gas interface propagation from one branch to two adjacent branches arises for certain combinations of flow direction and contact angle.

To illustrate the issue we will first discuss what would happen if the process discussed earlier – filling of a T-junction from *branch 1* – would be implemented using standard channel models as branches. In the second part, we will present the necessary modifications to allow for robust simulation of capillary pressures in T-junctions.

In the case of an empty T-junction getting wetted through capillary pressure by a liquid of contact angle < 90°, a numerical stability issue arises in the capillary pressure interpolation process after the first branch has filled and the two subsequent branches start filling. At this point the capillary pressure in direction of the flow increases linearly with the filled length of the branches (as long as the filled length is below the distance d_{cap}). As minute differences in the filled length of the two filling branches necessarily occur due to the numerical limitation of the precision of computation, one of the channels will be filled more than the other. Due to the higher capillary pressure in the channel with more liquid, an increasing liquid transfer from the channel with less liquid to the channel with more liquid will occur. This positive feedback mechanism for the liquid flow towards the branch with more liquid leads to the emptying of the branch with less liquid. In the instant when the channel with less liquid is emptied, a not considered case occurs as this corresponds to the formation of a gas plug, although the physically correct behavior would be filling of both branches.

The positive feedback in capillary channel filling during interpolation that is responsible for this instability occurs in two cases:

1) Wetting of an empty T-junction by capillary pressure (contact angle < 90°)
2) Emptying of a full T-junction by capillary pressure (contact angle > 90°)

In the other two cases

3) Wetting of an empty T-junction despite capillary pressure (contact angle > 90°)
4) Emptying of a full T-junction despite capillary pressure (contact angle < 90°)

the capillary pressure interpolation at the transition from one branch emptying/filling to two branches emptying/filling leads to a negative feedback which stabilizes the simulation against numerical imprecisions.

In order to overcome this problem, the branch models were modified in order to lead to a negative feedback in all cases by reversing the sign of the capillary pressure in the branches for the cases 1) and 2). This solves the stability issue but by itself leads to a stop of the processes 1) and 2). To compensate for this modification, an additional control pressure $p_{control}$ was introduced that acts in the direction of flow in the branch models depending on the wetting state of the logic block and the contact angle.

The procedure for the adjustment of $p_{control}$ is discussed in the following again for the process of an empty T-junction filling from *channel 1* – see S-Figure 3. If the liquid/gas interface has reached a distance from the boundary between *channel 1* and *branch 1* of less than d_{cap}, this leads to the interpolation from the wetting capillary pressure in *channel 1* to the de-wetting capillary pressure in *branch 1*. To compensate this – i.e. to maintain the overall physical behaviour of a constant capillary pressure inside the T-junction – the logic-block uses the same signal that is used for the interpolation - $MenT_{out\,1}$- between *branch 1* and *channel 1* to linearly increase the pressure $p_{control\,1}$ in *branch 1* in the direction of flow. In the first half of the unaltered capillary pressure interpolation, the sum of the capillary pressures of *channel 1* and *branch 1* drops to zero as the capillary pressure of *channel 1* $p_{cap\,1}$ is equal to $-p_{cap\,1}$ of *branch 1*. Therefore $p_{control\,1}$ is increased to $p_{cap\,1}$ in this first half of the interpolation. In the second half of the interpolation, the sum of the capillary pressures drops to the negative of the real capillary pressure which is compensated by increasing $p_{control\,1}$ to $2 * p_{cap\,1}$. Therefore, the effective capillary pressure is maintained throughout the capillary interpolation from *channel 1* to *branch 1*.

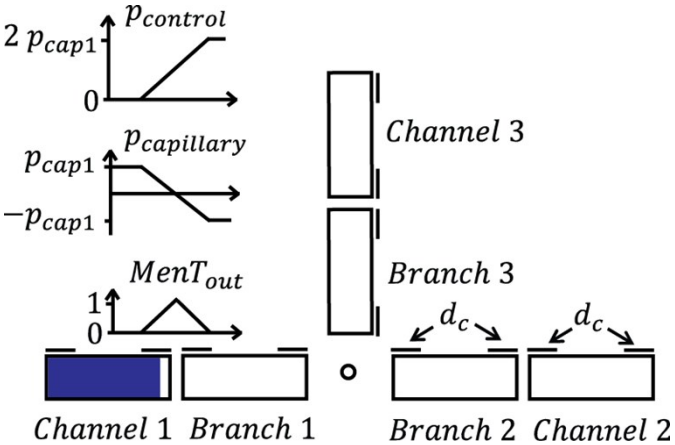

S-Figure 3: Illustration of the processes implemented to allow for robust capillary pressure handling at T-junctions. At the transition point between *channel 1* and *branch 1* the values of the meniscus position signal $MenT_{out\,1}$ of *channel 1* & *branch 1* are depicted for all the positions in the capillary pressure interpolation distance d_{cap} together with the corresponding values of the capillary pressure and the control pressure. As described in the main text, the effective capillary pressure is the sum of the indicated capillary pressure and control pressure and is constant during the liquid/gas interface transition.

As illustrated in S-Figure 4, this control pressure of $2 * p_{cap\,1}$ in *branch 1* is maintained until the T-junction has filled completely. Thereby, the transition of the liquid/gas interface from *branch 1* to *branch 2 & 3* is numerically stable and at the same time models capillary self-priming. As soon as the first of the two filling branches, e.g. *branch 2*, starts the capillary pressure interpolation with the connected *channel 2*, the generated overpressure is compensated by increase of the control pressure $p_{control\,2}$. This compensates the effect of $p_{control\,1}$ as all control pressures are directed from the distal side of the T-junction to the center of the T-junction. As soon as all branches are completely filled and the capillary pressure interpolation with all connected channels is completed, the values of $p_{control}$ is at $2 * p_{cap\,1}$ for all branches. The last step is the transition of the logic-block to the "completely filled T-junction" state in which all $p_{control}$ are set to zero.

Again, this process is implemented symmetrically in order to allow for filling or emptying with wetting or de-wetting contact angles from arbitrary channels.

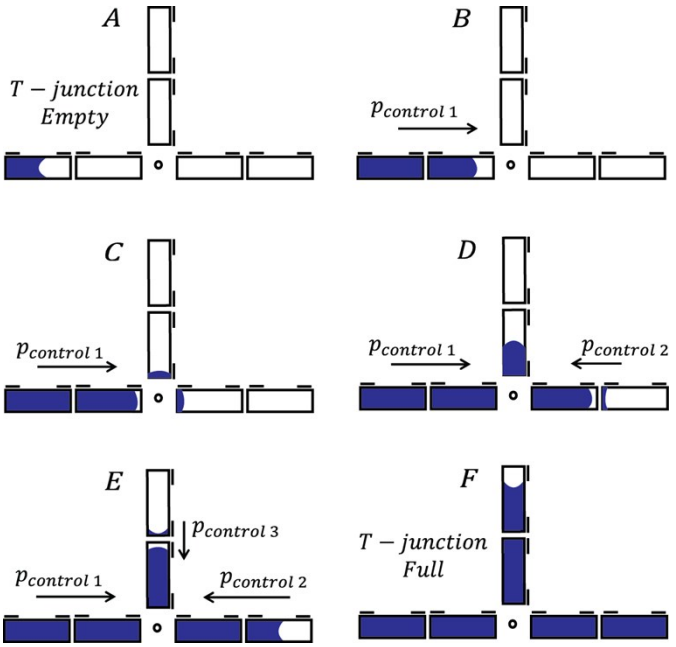

S-Figure 4: Illustration of the capillary pressure handling in a T-junction model block. Analogous to the illustrations for "capillary pressure interpolation at model block boundaries" the menisci indicate the direction and magnitude of the capillary pressure – not the actual fill level in the branches or channels. **A:** The fill level of *channel 1* is outside of the capillary pressure interpolation distance d_{cap}. The capillary pressure is therefore at the full value of the capillary hysteresis model. **B:** The transition from *channel 1* to *branch 1* has occurred as described in S-Figure 3. Therefore, the control pressure $p_{control\,1}$ is at its maximum value of $2 * p_{cap}$ in the direction towards the T-junction center and the capillary pressure in *branch 1* is at $-p_{cap}$. **C:** The capillary pressure interpolation at the transition point from *branch 1* to *branch 2 & 3* is under way. Due to the de-wetting capillary pressure in the branches, the transition is stable against numerical errors. **D:** The propagated fill level in *branch 2* leads to the capillary pressure interpolation between *branch 2* and *channel 2*. Therefore, the capillary pressure changes from de-wetting to wetting and the control pressure $p_{control\,2}$ is increased accordingly to compensate $p_{control\,1}$. **E:** The transition between *branch 2* and *channel 2* is completed and the transition between *branch 3* and *channel 3* is under way. **F:** After all branches have been filled and the meniscus tracking signals indicate that the capillary pressure interpolations are all finished, the logic case of the T-junction is changed to "full" and the control pressures are all set to 0.

S 4.3 Considered forces at T-junctions

The concept behind the T-junction model is to link the connected channel or chamber model blocks and allow for correct liquid filling behaviour. For this reason, wetting state propagation and capillary pressures are mandatory features. The remaining forces i.e. Centrifugal, Euler, Inertial and Coriolis pressure as well as viscous dissipation are not considered. For

centrifugal, Euler and inertial pressure, these omissions do not have an impact, because the idealized T-junction model does not have a physical extent and therefore these pressures are handled by the connected channels. The rationale behind the remaining idealizations is as follows:

The physical extent of the T-junction corresponds to the channel diameters of the connected channels. Therefore, the correction of the viscous dissipation at the T-junction, due to the potentially complex flow patterns, is considered to be negligible when compared to the absolute viscous dissipation of the connected channels. This includes the omission of enhanced viscous friction due to Dean flow and Coriolis force. If this idealization is not applicable, resolved 3D-CFD calculations of the flow resistance are recommended.

The omission of the Coriolis force has two reasons.

1) If liquid flows from an inlet channel into a T-junction and is distributed to two connected liquid-filled outlet channels, the pressure between the two outlet channels – generated by the Coriolis force – is highly dependent on the geometry of the T-junction and the resulting 3D flow pattern.
2) In cases where Coriolis switching[4] is performed at T-junctions, in addition to 1), the impact of the free liquid-gas interface on the liquid flow from the inflow path to the outflow path would need to be considered in order to correctly describe the acting Coriolis force and the capillary pressure at the partially filled T-junction would need to be modeled in order to avoid the generation of gas plugs which cannot be modelled in the simulation.

Therefore lumped model simulation of these effects is beyond the scope of this work and they are consequently neglected in lumped models of T-junctions. If the Coriolis force at a T-junction has a significant impact on the system dynamics – for example if a Coriolis switch is implemented – it is recommended to develop a specialized lumped T-junction model which considers Coriolis forces based on 3D-CFD simulations of the specific geometry of interest.

S5 Euler pressure in chamber models

The calculation of the Euler pressure in chambers is based on the approximation of a constant liquid filled isoradial length L_i if liquid is present in a chamber. With this approximation, the Euler pressure increases linearly from 0 at the right chamber wall to its maximum value on the left chamber wall in case of positive angular acceleration $\dot{\omega}$ (counter clockwise acceleration). For negative angular acceleration, the Euler pressure increases from 0 at the left chamber wall to its maximum at the right chamber wall – see S-Figure 5. The Euler pressure that is exerted on connected models is therefore dependent on the position of the connection. The parameter G is used to specify this position – see S-Table 3.

S-Table 3: Euler pressure approximation in chamber models. The position parameter G needs to be set to 1 for a model connection on the right side of a chamber and -1 if a model is connected on the left side. Between these two positions G is adjusted accordingly.

$\dot{\omega} > 0$	$\dot{\omega} \leq 0$
$p_{euler} = -\rho\, L_i\, \dot{\omega}\, r\, (G-1)/2$	$p_{euler} = \rho\, L_i\, \dot{\omega}\, r\, (G+1)/2$

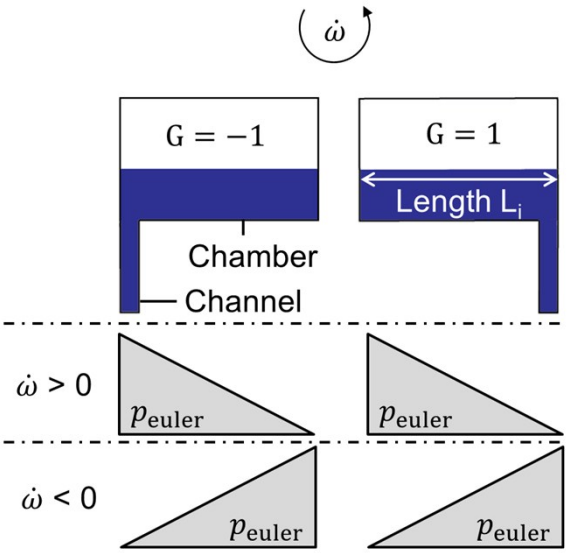

S-Figure 5: Illustration of the Euler force approximation for chamber models. If a channel model is connected to the chamber on the left side of the chamber, the position parameter is $G = -1$. On the right side $G = 1$ applies. Intermediate positions are interpolated linearly. The grey illustrations of p_{euler} indicate the Euler pressure as a function of the position parameter **G** for the two directions of angular acceleration.

S6 Controller models

The concept behind the use of controller models is to use the available information about the system dynamics during simulation to automatically derive the correct operation procedure to reach a desired system behavior. The chosen example is the determination of the appropriate spin protocol for a constant flow rate inside a channel. The rotation frequency of the system is therefore adjusted during simulation through the following equation:

$$f = 10^4 \frac{1}{s\,\mu l}(q_t - q(t))$$

If the resulting frequency change rate exceeds the capabilities of the experimental setup (30 Hz/s), the frequency change rate is limited to that value. Due to the direct influence of the frequency on the – flow driving – centrifugal force, the rate of frequency change is chosen proportional to the deviation between the desired flow rate q_t and the actual flow rate in every given instant $q(t)$. The high gain-factor of 10^4 describes how fast the frequency is adjusted in case of a deviation between target flow rate and actual flow rate.

This simple equation can be used to control the flow rate in the channel for two reasons.

First: Due to the limitation of the allowed acceleration to 30 Hz/s, physical effects that lead to a phase-shifted response of the system – such as inertial pressures or fluidic capacities –

have a small magnitude when compared to the centrifugal force, which is controlled in a time-lag free manner via the spin frequency. Therefore, the high gain factor for the frequency change does not generate large delayed effects that would lead to unstable control behaviour and oscillations in the flow rate. On the other hand it does lead to a fast response of the frequency, if the flowrate deviates from the target value.

Second: Implicit solvers for stiff differential-algebraic systems – used for network simulation in centrifugal microfluidics – are able to detect the onset of oscillations during a simulation and refine their time-step as needed in order to keep the simulation result within a specified numerical error tolerance. This feature allows the use of high gain factors and simple control equations as explained in the following: If a solver uses a fixed finite time step for the integration of the system equations, this time step corresponds to the time between two "measurements" of the quantity to be controlled. In the time between the "measurements", the controller adjusts the control parameter – here the rotation frequency – according to the last "measurement". If the gain factor of this adjustment and the time step are too large, the controlled quantity – here the flow rate – overshoots within the time between "measurements" and the controller needs to react in the opposite direction in the next time step. By automatically reducing the time step, the used solvers avoid the oscillations that would result from this "measurement" time-lag and thereby allows for large gain-factors.

In summary, controller models in centrifugal microfluidic network simulations offer the following advantages: They

1) are simple to implement*
2) can be implemented in any microfluidic element model
3) allow for the control of any parameter that influences system behaviour
4) can be simulated fast
5) are robust against solver induced controller oscillations

* If the boundary condition is met, that the physical system dynamics is dominated by a force that is controlled by the control parameter. Otherwise more general PID controllers need to be applied or the corresponding additional physical effects need to be taken into account within the controller model.

S7 Coriolis effect on flow resistance

S 7.1 Comsol simulation study of flow resistance

Haeberle et. al. describe, that if liquid flows in a microfluidic channel on a rotating disc, the Coriolis force leads to a transversal convection of liquid from the center of the channel to one of its walls[5]. In addition to the described resulting liquid folding effect, this leads to an increase of the liquid velocity gradient at said wall and thereby increases the viscous dissipation of the channel. In current lumped models for network simulation in centrifugal microfluidics, this effect is neglected.

To the best of our knowledge, the impact of this effect on the effective flow resistance of channels in centrifugal microfluidics has not yet been characterized. Therefore – due to the complex 3D structure of the flow distortion that generates this additional viscous dissipation – we calculate the maximum error introduced by the omission of this effect by 3D – CFD simulations using COMSOL Multiphysics® 5.1 (www.comsol.com, 2015). As model, liquid water at 20°C was chosen (viscosity: 1 mPas; density 1000 kg/m^3). The calculation domain was defined as a water filled channel with square cross-section (length of 1 cm; three different channel cross-sections as used in the design of this publication's fluidics: 200 µm x 200 µm, 300 µm x 300 µm, 400 µm x 400 µm). The domain was meshed according to the recommended standard, physics-controlled setting in COMSOL (free tetrahedral mesh, two boundary layers at the channel walls). The boundary conditions were set to no-slip at the channel walls, ambient pressure at the outlet and a pressure at the inlet according to the expected pressure drop induced by viscous dissipation in the channel at a given ideal Hagen–Poiseuille volume flow. This pressure drop was calculated by the formula for viscous dissipation as depicted in Table 1. A grid independent test was performed (S-Table 4) by repeatedly increasing mesh resolution and calculating the stationary solution for the average volume flow in the channel.

S-Table 4: A grid independent test was performed by evaluating the case study of a water-filled channel (length: 1 cm; cross section 200 µm x 200 µm). The inlet was set to 16005.5 Pa and the outlet to ambient pressure, which corresponds to 90 µl/s flow rate in the channel when assuming and analytically calculating an ideal Hagen–Poiseuille volume flow. The number of elements in the domain was increased step by step. At each step, the respective stationary solution of the flow rate was calculated and compared to the step before. At approximately 1.2 million domain elements, the mesh was deemed to be sufficiently resolved as solutions between steps, both with and without Coriolis force only displayed slight changes.

Domain elements	Flow rate in 200µm x 200µm channel without Coriolis force [µl/s]	Flow rate in 200µm x 200µm channel with Coriolis force [µl/s]
41500	84.9	73.5
81271	87.5	74.4
226715	88.7	74.3
451733	89.6	74.2
1178028	89.8	74.2

At approximately 1.2 million domain elements (200 µm x 200 µm channel) both the COMSOL simulation and the analytically calculated values resulted in close to identical average volume flows (S-Table 4) and thus, the mesh was deemed to be sufficiently resolved. The Coriolis force was modeled as a force that is applied to each domain element. Absolute value and

direction of this force is calculated in dependency of the element's velocity vector as well as rotational frequency and rotational direction of the disc. The stationary solution is calculated (Example depicted in S-Figure 6). Flow rates with and without Coriolis force are compared. As expected, the Coriolis force leads to a decrease in flow rate."

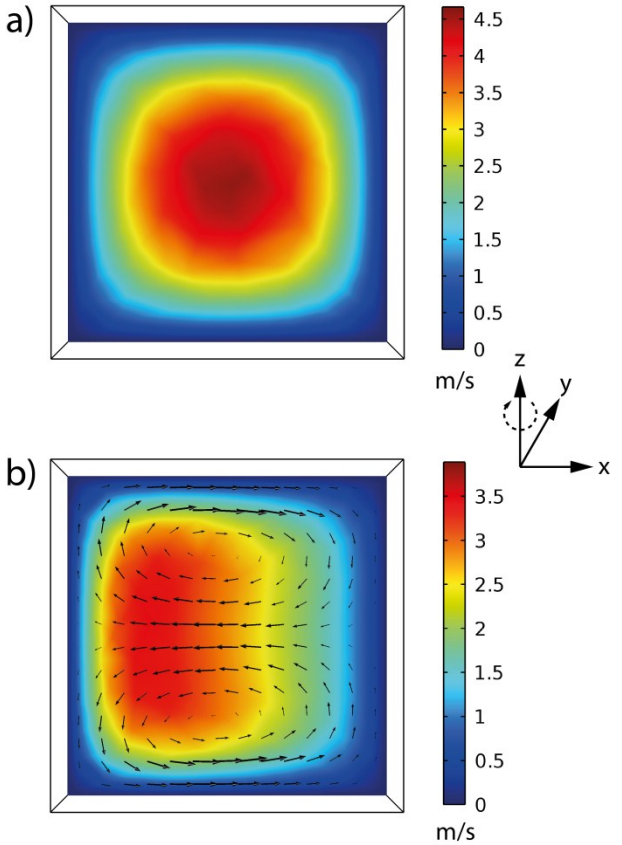

S-Figure 6: Flow velocity distribution in the cross section of a 200 µm x 200 µm channel on a disc rotating at 60 Hz (z is the rotational axis, the disc is rotating in clockwise direction). Boundary conditions: inlet: 16005.5 Pa; outlet: 0 Pa. The main direction of the volume flow is in y-direction away from the center of rotation. **a)** In color: distribution of the y-component of the velocity field if the Coriolis force is neglected. As expected, an ideal Hagen–Poiseuille flow with a flow rate of 89.8 µl/s is observed. **b)** In color: distribution of the y-component of the velocity field if Coriolis force is considered. This leads to a distorted Hagen-Poiseuille flow profile, higher viscous dissipation and thus a lower overall flow rate in the channel of 74.2 µl/s and cross currents depicted by arrows (The arrows length is proportional to the flow velocity; the largest arrows correspond to 0.3 m/s).

In general, the effect increases with flow rate and angular velocity of the disc[6], therefore, the calculations were performed for the highest flow-rates and angular velocities occurring during the different fluidic steps of the mixing and valving process. The results are compiled in S-Table 5 and discussed in the following subsections.

S-Table 5: Increase in flow resistance due to Coriolis force in channels. The maximum flow rates predicted by network-simulation for the different fluidic operation steps were used for the resolved CFD simulations.

Channel dimensions	Rotation Frequency	Flow rate network-	Flow rate in COMSOL	Resistance increase
w [µm] x d [µm]	[Hz]	simulation without Coriolis force [µl/s]	with Coriolis force [µl/s]	[%]
200 x 200	60	90	74.21	17.55
200 x 200	60	70	59.10	15.57
300 x 300	40	0.6	0.57	4.93
300 x 300	30	62	54.08	12.77
300 x 300	20	0.5	0.49	1.42
300 x 300	10	6	5.97	0.46
300 x 300	8	5.5	5.48	0.29
400 x 400	57	3.5	2.87	17.91
400 x 400	40	75	58.90	21.46
400 x 400	40	40	33.27	16.83
400 x 400	30	110	87.97	20.03

S 7.2 Step 1: Loading

During the initial transfer of liquid from the *inlet* to *pneumatic chamber 1* through the inlet channel, the rotation frequency increases first from 0 Hz to 10 Hz with 3 Hz/s and thereafter to 60 Hz with 15 Hz/s. In combination with the large radial extent of the connecting channel (dimensions: 200 µm x 200 µm) this leads to a ramp up of the flow rate to ~ 70 µl/s in the network-simulation prediction, see S-Figure 7.

The CFD-simulation result for the resistance increase under the maximum conditions is 15.57 % resulting in a reduction of the effective flowrate to 59.10 µl/s.

Because the flow-rate during transfer is on average well below 70 µl/s, the error in flow resistance is on average also well below 15.57 %. In combination with the fact that this resistance increase only leads to a small delay in the transfer, this explains why the fill levels in *pneumatic chamber 1* and *mixing chamber* correspond to the simulation predictions within the measurement tolerances.

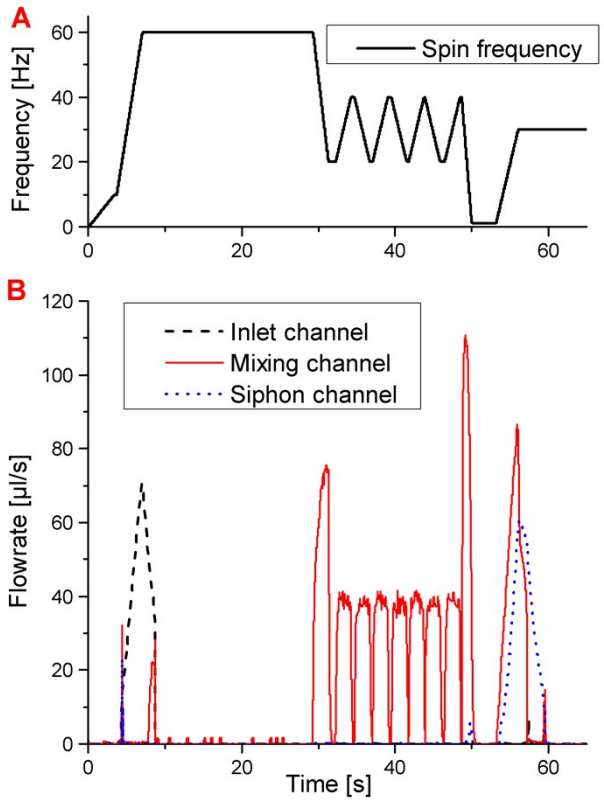

S-Figure 7 A: Frequency protocol used during experiments with water, as described in the main paper. **B:** Corresponding predictions of the absolute values of the flow rates in the inlet channel, the mixing channel and the siphon channel. The highest increase of the fluidic resistance in channels due to Coriolis force is to be expected for high flow rates and high spin frequencies. The corresponding cases are discussed in the main text.

S 7.3 Step 2: Mixing

During the initial deceleration step from 60 Hz to 20 Hz with 20 Hz s^{-1}, the flow rate in the mixing channel (dimensions: 396 µm x 391 µm) reaches 75 µl/s at < 40 Hz. In the following mixing cycles, the flow rate oscillates between + 40 µl/s and 0 µl/s at a maximum rotation frequency of 40 Hz, see S-Figure 7.

The corresponding CFD-simulation results for the maximum resistance increase under these conditions are 21.46 % for 75 µl/s and 16.83 % for 40 µl/s respectively.

During the mixing steps, the pressure drop due to viscous dissipation in the channels between pneumatic chamber 1 and mixing chamber is therefore predicted by network simulation to < 1370 Pa (initial deceleration) and < 730 Pa (subsequent mixing). As the pneumatic pressure built up in the pneumatic chamber varies continuously between 7700 Pa (20 Hz) and 20200 Pa (40 Hz), the viscous dissipation is small compared to the driving centrifugal pressure. Therefore, a deviation in the viscous dissipation only leads to a small lag of the liquid flow between *mixing chamber* and *pneumatic chamber 1* that cannot be detected within the measurement tolerances.

The maximum flow rate predicted in the *siphon channel* during mixing is 0.5 µl/s at 20 Hz, leading to a pressure loss due to viscous dissipation of 2 Pa. The corresponding fluidic resistance increase is 1.42 %. In comparison to the contributions of the centrifugal (8000 Pa) and capillary (270 Pa) pressure, this effect is therefore negligible.

S 7.4 Step 3: Valving

The flow rate in the siphon channel during valving reaches 5.5 µl/s at 8 Hz which corresponds to 22 Pa pressure loss due to viscous dissipation. The simulated flow resistance increase is 0.29 %. Again, the centrifugal pressure of the liquid column of the completely filled siphon channel (3400 Pa in the moment of siphon crest priming) and the capillary pressure (270 Pa) are the barriers that need to be overcome to prime the siphon. Therefore the additional pressure drop due to the fluidic resistance increase is also negligible for the outcome of the valving process.

S 7.5 Step 4: Transfer

During transfer, the network-simulation predicted flow rate in the siphon channel reaches 62 µl/s at 30 Hz. Therefore the simulated maximum flow resistance increase is 12.77 % which leads to a predicted flow rate reduction to 54.08 µl/s. This effect lies within the measurement tolerances and was not detected.

S 7.6 Discussion & Outlook

Though the increase of viscous dissipation caused by a distortion of the flow profile by the Coriolis force is negligible for the discussed configuration, it might be important in other settings. Namely all cases where the flow rates of liquids on centrifugal systems need to be known with high precision. One example might be to achieve a certain flow rate in a channel with high fluidic resistance through time-dependent strong centrifugation. Another example might be mixing of two fluids inside a channel due to the discussed Coriolis induced liquid folding effect. Here, the ratio of the flow rates of the liquids to be mixed needs to be precisely defined and could be controlled by the spin frequency.

The impact of the Coriolis force on the viscous dissipation of Newtonian liquids can possibly be modeled in the future by an empirical function of the following variables: flow rate, geometry, channel dimensions and spin frequency.

Equipped with the means to correctly predict the fluidic resistance of fast flows under high centrifugation we expect the network simulation approach to allow for an even wider range of applications.

S8 Liquid property influence on pumping & valving

S 8.1 50% ethanol in DI water w/w

Due to the small advancing and receding contact angles of 52.5° and 30°, respectively, ethanol shows a highly wetting behavior. This leads to a destabilization of the siphon valve. In order to avoid premature priming, the 1st deceleration from 60 Hz to 20 Hz was therefore adjusted from 20 Hz s^{-1} to 10 Hz s^{-1}.

In all other features the used frequency protocol depicted in S-Figure 8 A is identical to the frequency protocol used for water. In S-Figure 8 B the measured volumes in the mixing chamber are systematically approximately one standard deviation above the simulation predictions. A possible explanation of this result lies in the highly wetting behavior of ethanol which also wets the chamber walls and therefore can lead to a systematically too high measured fill level. S-Figure 8 C shows the liquid volume inside the pneumatic chamber 1 during processing. Here the simulation predictions and experimental results match closely. The liquid fill levels in the siphon channel show excellent agreement between experiment and simulation as can be seen in S-Figure 8 D for the processing phase with closed valve as well as for the valving process.

S 8.2 50% glycerol in DI water w/w

Due to the high viscosity of the glycerol solution, the viscous dissipation in the channel increases and as a result the flow rates during disc processing are reduced. To ensure complete transfer of the liquid from the inlet chamber to *pneumatic chamber 1* the hold time at the loading frequency of 60 Hz has been increased (see S-Figure 9 A). In S-Figure 9 B the liquid volume in the mixing chamber is depicted with the simulation predictions based on the frequency protocol used during experiments. The reached liquid volume plateau at t = 25s indicates the completion of the liquid transfer step from the inlet chamber to the pressure chamber 1 and mixing chamber. The impact of the increased viscosity can also be seen in the slower decrease of the liquid volume in the mixing chamber after valving, i.e. between t=55s and t=70s. S-Figure 9 C shows the excellent agreement between the fill levels in pneumatic chamber 1 and the corresponding simulation predictions. S-Figure 9 D shows the same excellent agreement for the siphon fill levels during processing.

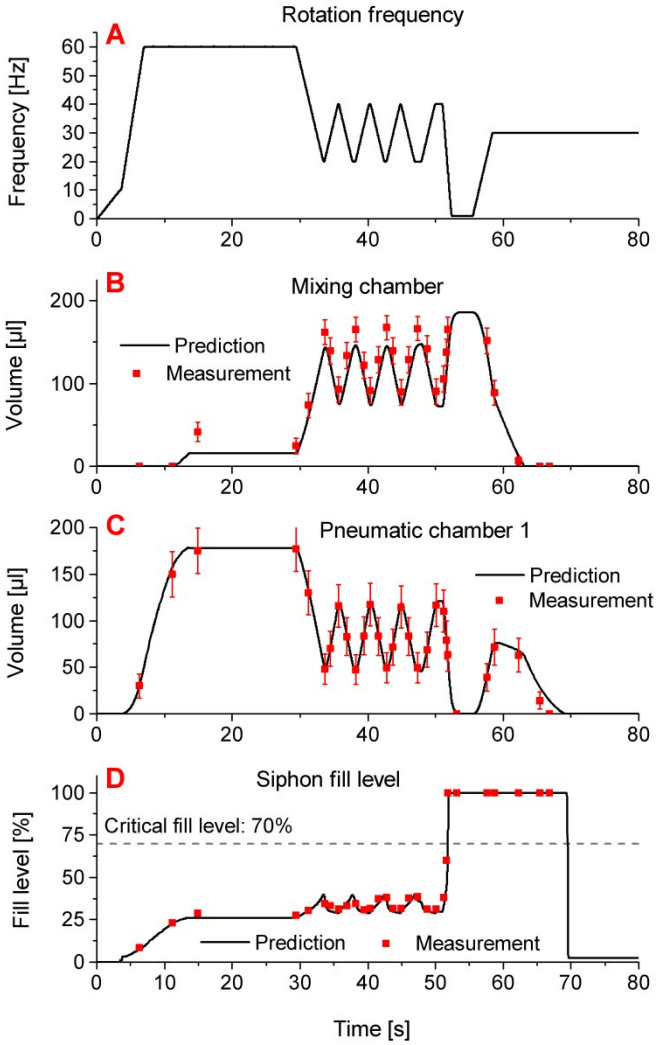

S-Figure 8: **A:** Spin protocol of system operation during experiment with 50% ethanol in water solution. **B&C:** Liquid volumes inside *mixing chamber* and *pneumatic chamber 1* during system operation. The black continuous line corresponds to the simulation prediction based on the spin protocol in A. The red dots indicate experimental results. The error bars correspond to the sum of the measurement accuracy of the fill levels in the respective chambers and the expected volume error based on manufacturing tolerances of the chambers. **D:** Siphon fill levels as indicated in Figure 3 of the main paper. If the liquid fill level exceeds the critical fill level, the final increase in spin frequency leads to liquid transfer to the downstream fluidics.

S 8.3 Blood plasma

In S-Figure 10 the results of the experiments with blood plasma are depicted together with the simulation predictions, which were again based on the frequency protocol used in the experiments (S-Figure 10 A). In order to be able to process blood plasma the spin frequency after triggering the siphon valve was reduced from 30 Hz to 10 Hz. This is was necessary, because during liquid transfer to the downstream fluidics an underpressure occurs at the siphon crest which leads to degassing of blood plasma. Therefore the transfer is stopped if a spin frequency of 30 Hz is used. All other features of the spin protocol are identical to the frequency protocol used for processing of water. The volumes of blood plasma in the

Mixing chamber, depicted in S-Figure 10 B, show excellent agreement with the simulation predictions. The reduced speed of liquid transfer at 10 Hz, when compared to liquid transfer at 30 Hz in used with the other liquids, can be seen in the comparably slow decrease in the liquid fill level in the mixing chamber between t = 55s and t = 80 s. The liquid fill level in pneumatic chamber 1 (S-Figure 10 C) also reflects the low rotation speed during this timeframe as the reduced centrifugal pressure is compensated by a smaller amount of gas compressed by the liquid in pneumatic chamber 1. The fill levels in the siphon channel (S-Figure 10 D) show again excellent agreement between simulation and experiment. We would like to point out that the coating behavior of blood plasma was taken into account in the simulations.

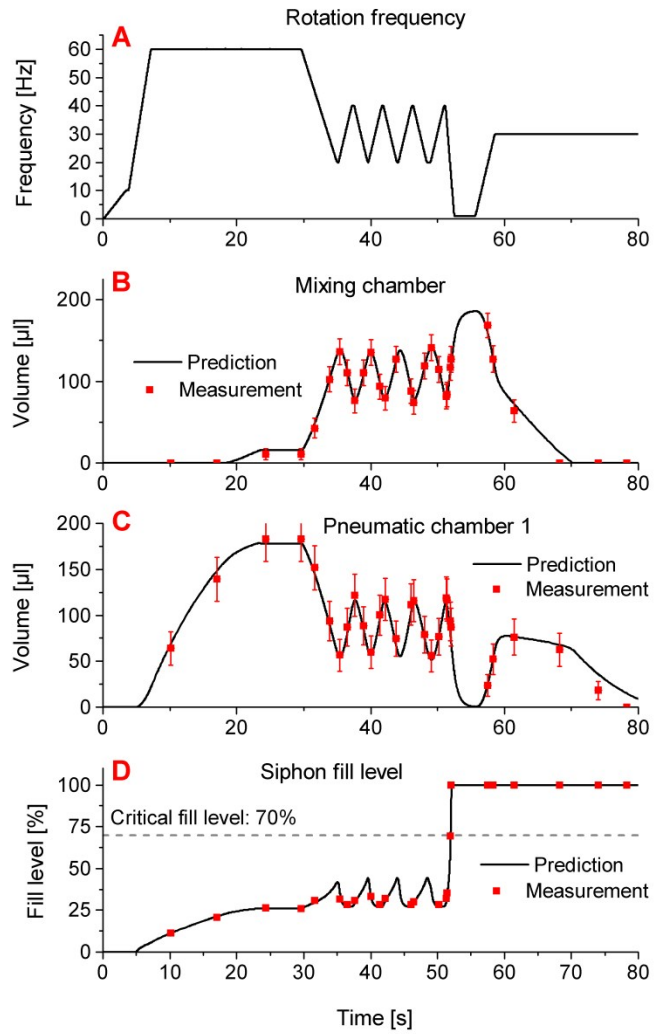

S-Figure 9: System behaviour in analogy to **S-Figure 8** for 50% glycerol in water solution.

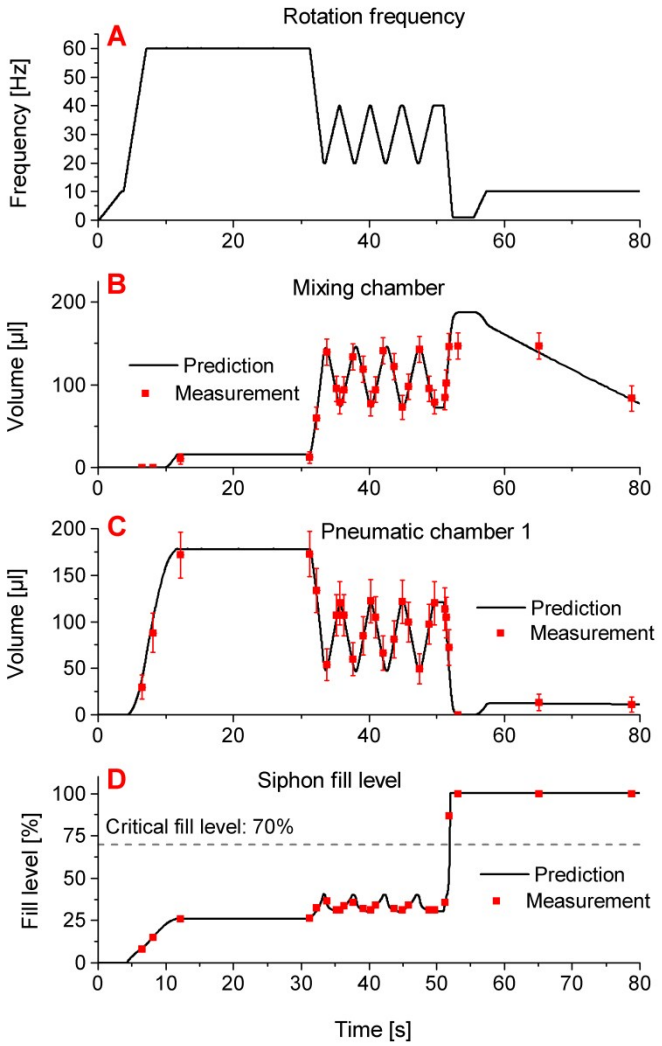

S-Figure 10: System behaviour in analogy to **S-Figure 8** for blood plasma.

S9 Fluidic resistance of rectangular channel

In this section we would like to provide the error estimation for the formula used in Table 1 of the manuscript for the fluidic resistance of a rectangular channel. We start with the exact fourier-series expression for the fluidic resistance as given by Bruus [2]:

$$R_r = \frac{12\,\eta\,L}{h^3 w\left(1-\frac{192\,h}{\pi^5\,w}\left(\sum_{n=1}^{\infty}\frac{1}{(2n-1)^5}\tanh\left(\frac{(2n-1)\pi w}{2h}\right)\right)\right)}$$

As we need to truncate the infinite series S in the denominator we will derive a simplified approximation for

$$S = \sum_{n=1}^{\infty} \frac{1}{(2n-1)^5} \tanh\left(\frac{(2n-1)\pi w}{2h}\right)$$

$$tanh(x) = \frac{e^x - e^{-x}}{e^x + e^{-x}}$$

Since quickly approaches 1 with increasing argument x the higher terms in the series, i.e. for n > 1 are already very close to 1. The minimal value of $\tanh\left(\frac{(2n-1)\pi w}{2h}\right)$ is always found for w=h, therefore we choose an approximation of S using w=h which leads to an overestimation of the error for all other aspect ratios h/w<1. This approximation of S is found by using the relation

$$tanh(x) = \frac{e^x - e^{-x}}{e^x + e^{-x}} = 1 - \frac{2e^{-x}}{e^x + e^{-x}} > 1 - 2e^{-2x} \quad \text{for } x > 0$$

The argument in S is $x = \frac{(2n-1)\pi w}{2h}$ which is > 0 for all $n > 0$ and minimal for $h = w$. Therefore the maximal error by approximating $tanh(x)$ by 1 is $2e^{-2x}$ which is $2e^{-(2n-1)\pi}$ for an element in S with summation index n.

By separating the first term of the series expansion and approximation of the remainder we get:

$$S = \tanh\left(\frac{\pi w}{2h}\right) + \sum_{n=2}^{\infty} \frac{1}{(2n-1)^5} \tanh\left(\frac{(2n-1)\pi w}{2h}\right)$$

$$\approx \tanh\left(\frac{\pi w}{2h}\right) + \sum_{n=2}^{\infty} \frac{1}{(2n-1)^5}$$

Using

$$\sum_{n,\,odd}^{\infty} \frac{1}{(n)^5} = \sum_{n=1}^{\infty} \frac{1}{(n)^5} - \sum_{n,\,even}^{\infty} \frac{1}{(n)^5}$$

$$= \zeta(5) - \sum_{k=1}^{\infty} \frac{1}{(2k)^5} = \zeta(5) - \frac{1}{32}\zeta(5) = \frac{31}{32}\zeta(5)$$

This leads to

$$S_{approx} = \tanh\left(\frac{\pi w}{2h}\right) + \left(\frac{31}{32}\zeta(5) - 1\right)$$

With the Riemann Zeta function ζ.

A sufficiently accurate approximation of the approximate value of $\zeta(5)$ ([7]) is 1.036925577

According to the derivation above, the error E of this approximation of S can itself be approximated by

$$E < \sum_{n=2}^{\infty} \frac{1}{(2n-1)^5} 2e^{-(2n-1)\pi}$$

$$< \frac{2}{(3)^5} \sum_{n=2}^{\infty} e^{-(2n-1)\pi}$$

$$= \frac{2}{243} \sum_{n=2}^{\infty} e^{-(2n-1)\pi}$$

$$= \frac{2}{243} e^{-2\pi} \sum_{n=1}^{\infty} \left(e^{-n\pi} - e^{-2n\pi}\right)$$

$$= \frac{2}{243} e^{-2\pi} \left(e^{-\pi} \frac{1}{1-e^{-\pi}} - e^{-2\pi} \frac{1}{1-e^{-2\pi}}\right)$$

$$< 6.66 * 10^{-7}$$

The resulting maximal relative error $R_{r,\,err,\,rel}$ of the resistance calculation is

$$R_{r,\,err,\,rel} = \frac{1}{R_r} \frac{\partial R_r}{\partial S} E = \frac{\frac{192\,h}{\pi^5\, w} E}{1 - \frac{192\,h}{\pi^5\, w} S} < 1.14 * 10^{-6}$$

For the maximum aspect ratio h=w and the simplified worst case approximation of S by $\frac{31}{32}\zeta(5)$. Using S_{approx} in R_r leads to the formula

$$R_{\sim r} = \frac{12\,\eta\,L}{h^3 w \left(1 - \frac{192\,h}{\pi^5\, w}\left(\tanh\left(\frac{\pi w}{2h}\right) + \frac{31}{32}\zeta(5) - 1\right)\right)}$$

Which is used in the manuscript.

S10 Simulation results for pressures in fluidic network

In this section we would like to illustrate the pressure dynamics in the studied microfluidic network. S-Figure 11 A depicts the fluidic structure together with the positions for which the pressures (relative to the ambient) are given in S-Figure 11 C. The pressure data was obtained from the same simulation that was used for the comparison between experimental results and simulation predictions for processing of water – depicted in figure 10 in the manuscript. The frequency protocol for processing of the disk is shown in S-Figure 11 B.

1) In the illustration it can be seen that at the outlet of the *inlet chamber* (1) the pressure only increases shortly during the transfer phase due to the increasing centrifugal pressure. After emptying of the *inlet chamber*, the pressure remains constant at ambient pressure.
2) The pressure at the siphon crest (2) of the *inlet siphon channel* decreases below the ambient by up to 300 mbar during the initial liquid transfer from the *inlet chamber* to *pressure chamber 1*. This effect is a result of the falling liquid level in the *inlet chamber*, the centrifugal force acting on the liquid in the *inlet siphon channel* (on the rising and falling side) and the viscous dissipation of the resulting liquid flow.
3) The pressure at the radial outward end of the *mixing channel* reflects the pressure dynamics of the whole process. During the initial liquid transfer phase the pressure rises to the maximum centrifugal pressure of ~ 600 mbar. During mixing, the pressure varies,

mainly due to the change of the centrifugal pressure of the liquid column between the liquid level in the *mixing chamber* and (3).

4) The pressure in gas phase in *pressure chambers 1 & 2* (4) shows a similar behaviour as (3). In equilibrium the difference is given by the centrifugal pressure of the liquid column inside *pressure chamber 1*. The close following of the two curves shows that the pressures in (3), (4) and (5) are never far from equilibrium.
5) Pressure at the the radial inward outlet of the *mixing channel* (5). The pressure at this position is given by the centrifugal pressure of the liquid column inside the mixing chamber. The delay before the pressure increases to a value > 0 shows that the *mixing chamber* is only filled after the main liquid volume has been transferred to *pneumatic chamber 1*.
6) The pressure at the crest of the *siphon valve* (6) is constant at ambient pressure until the siphon valve is triggered. During the liquid transfer phase to the *downstream fluidics* the pressure decreases below ambient. As discussed for the inlet channel, the reasons are the falling liquid level in the mixing chamber and mixing channel, the centrifugal force acting on the liquid in the siphon valve channel and the viscous dissipation of the resulting liquid flow.

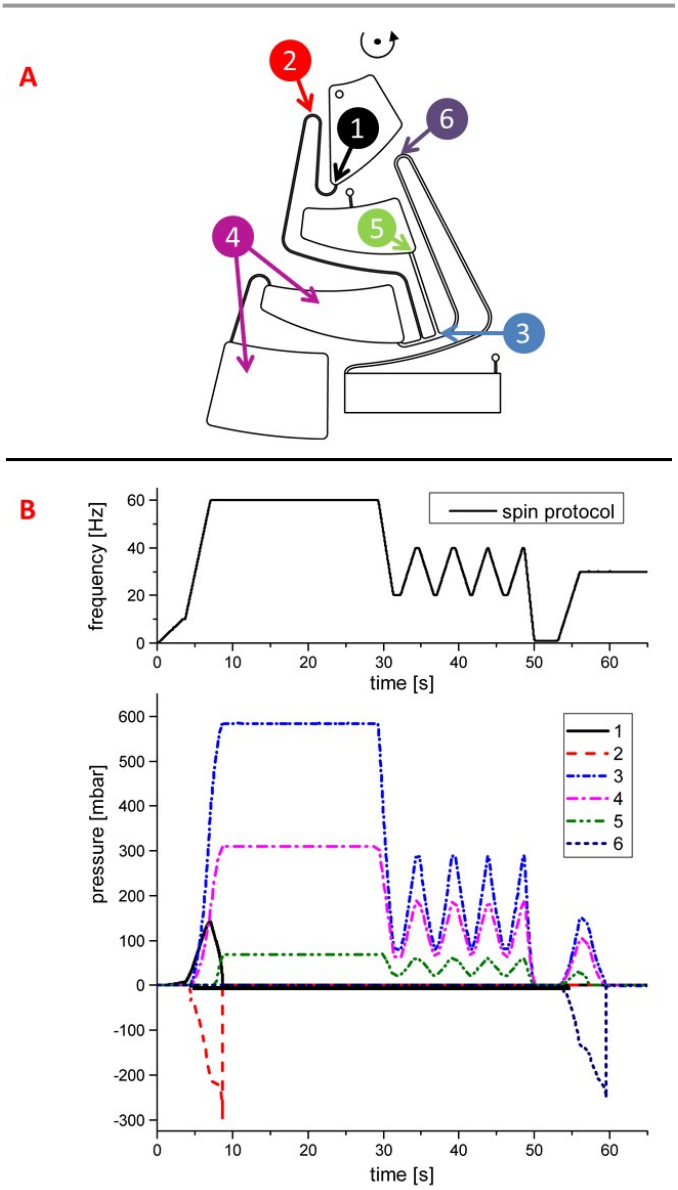

S-Figure 11: A) Illustration of selected positions for which simulation results for the pressure are given. **B)** Frequency protocol of processing used in the simulation. **C)** Simulation results of pressures – relative to ambient – at the positions illustrated in **A**. The simulation for the dynamics of water was used.

S11 Coriolis pressure in lumped chamber models

As lumped element models only need to correctly describe the through and across variables at their boundaries in order to yield correct simulation results, the Coriolis force is neglected in chamber models. In principle the Coriolis force can have an impact on the pressure at a chamber opening due to two effects. The first effect is an increased fluidic resistance of the chamber due to the secondary flow which has already been described for channels. As the fluidic resistances of chambers are negligible when compared to channels, the correction of the fluidic resistance is negligible as well.

The second influence on the pressure calculation can arise from flow patterns inside a chamber that lead to a direct Coriolis

pressure acting on the channel-chamber interface in the chamber. On the one hand the precise effect of the Coriolis force on the channel-chamber interface depends on the complex spacially resolved flow pattern inside the chamber and cannot be represented in generic lumped element models for chambers with arbitrary geometries. On the other hand the larger cross sections of chambers lead to correspondingly lower liquid flow velocities inside chambers when compared to the channels to which the chambers are connected. Therefore the Coriolis pressure can be neglected in chamber models when compared to channel models.

References

1 M. Bahrami, M. M. Yovanovich and J. R. Culham, *Transactions of the ASME*, 2006, **128**, 1036–1044.

2 H. Bruus, *Theoretical microfluidics*, Oxford University Press, Oxford, 2008, vol. 18.

3 Q. Wei et al., *Angew. Chem. (Int. Ed. in English)*, 2014, **53**, 8004–8031.

4 a) J. Kim et al., *Sensors and Actuators B: Chemical*, 2008, **128**, 613–621; b) T. Brenner et al., *Lab on a chip*, 2005, **5**, 146–150;

5 J. Ducrée et al., *Microfluid Nanofluid*, 2006, **2**, 97–105.

6 D. Chakraborty, M. Madou and S. Chakraborty, *Lab Chip*, 2011, **11**, 2823–2826.

7 M. Abramowitz and I. A. Stegun, eds., *Handbook of mathematical functions*, Dover Publ, New York, NY, 8th edn., 1972.